Peer-reviewed version available at *Appl. Sci.* **2019**, *9*, 4309; doi:10.3390/app9204309

Article

Systematic link of modal identification with model updating

Keunhee Cho, Young-Hwan Park, Jeong-Rae Cho*

Structural Engineering Research Institute, Korea Institute of Civil Engineering and Building Technology, 283, Goyangdae-Ro, Ilsanseo-Gu, Goyang-Si 10223, Gyeonggi-Do, Korea; kcho@kict.re.kr (K.C.); yhpark@kict.re.kr (Y.-H.P.)

* Correspondence: chojr@kict.re.kr; Tel.: +82-31-910-0663

Abstract: A systematic approach for model updating using the modal identification results is proposed. Modal identification provides mode shapes for physical quantities (acceleration strain, etc.) measured in specific directions at the location of the sensors. Besides, model updating involves the use of the mode shapes related to the nodal degrees-of-freedom of the finite element analytic model. Consequently, the mode shapes obtained by modal identification and the mode shapes of the model updating process do not coincide even for the same mode. Therefore, a method constructing transform matrices that distinguish the cases where measurement is done by acceleration, velocity and displacement sensors and the case where measurement is done by strain sensors is proposed to remedy such disagreement between the mode shapes. The so-constructed transform matrices are then applied when the mode shape residual is used as objective function or for mode pairing in the model updating process. The feasibility of the proposed approach is verified by means of a numerical example in which the strain or acceleration of a simple beam is measured and a numerical example in which the strain of a bridge is measured. Using the proposed approach, it is possible to model the structure regardless of the position of the sensors and to select the location of the sensors independently from the model.

Keywords: model updating; modal identification; measured data; measured mode shape

1. Introduction

In general, the model updating for a structure proceeds by minimizing the difference in the responses of the structure and of the model. The response of the structure can be physical quantities measured by sensors or be eigenvalues and mode shapes obtained by modal identification. Except the eigenvalues, the measured quantities and the mode shapes are values specific to the location of the sensors. Considering that the location of the sensors does generally not coincide with the mesh of the finite element model, it is necessary to perform a proper transform that make the location of the sensor match with the finite element model. Figure 1 shows the case where the location of the acceleration and strain sensors does not coincide with the position of the nodes in the model. In addition, the type of the measured physical quantities as well as the measurement direction shall be considered.

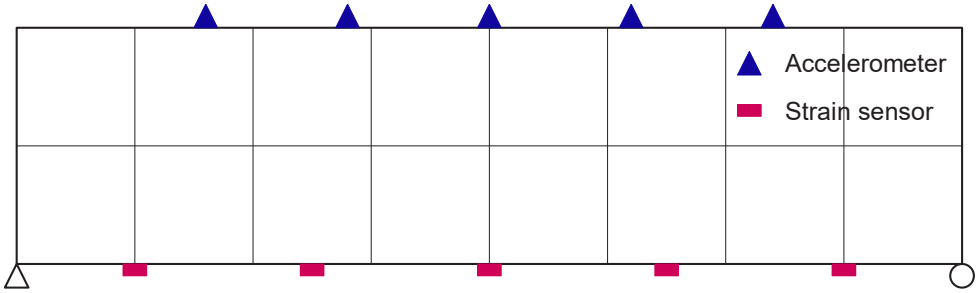

Figure 1. Mismatch of measurement location and finite element mesh.

The modal identification extracting the dynamic characteristics of the structure from the measured data can be done in both frequency domain and time domain. FDD (Frequency Domain Decomposition) [1] is a modal identification method in the frequency domain. ERA (Eigensystem Realization Algorithm) [2] and subspace identification method [3,4] are modal identification methods in the time domain. Such modal identification provides the natural frequencies of the structure at hand and the mode shapes for the measured physical quantities in the measurement direction at the location of the sensors.

The parameters of the numerical model can be derived by model updating using the so-obtained eigenvalues and mode shapes. The model updating methods can be divided into those relying on a deterministic approach [5,6] and those relying on a statistical approach [7-10]. The mode shapes obtained by eigen analysis in the model updating process are those related to the nodal degrees-of-freedom (DOF) of the analytic model and differ from the measured mode shapes obtained by modal identification. Accordingly, it is necessary to provide a solution to remedy such mismatch. Sanayei and Saletnik [11] introduced a transform matrix for the strain measurement to make the measured DOFs and model DOFs coincide and used the strain generated by static loading to perform model updating. Esfandiari *et al.* [12] defined a frequency response function for the strain to perform model updating. However, these studies are limited to the case where the measurement direction of the strain sensors coincides with the longitudinal direction of the member and cannot be applied for sensors installed in arbitrary directions.

The survey shows that numerous studies were implemented on modal identification or model updating but stresses also the scarcity of studies on methods linking these two processes. Consequently, the present study intends to propose a systematic approach linking the modal identification results to model updating. Section 2 derives a method achieving model updating using the data monitored by acceleration, velocity, displacement and strain sensors installed in arbitrary locations and directions in the structure. Section 3 explains the proposed approach through a simple numerical example. Section 4 verifies the feasibility and applicability of the proposed approach by means of a numerical example for a bridge structure.

2. Materials and Methods

2.1. Modal identification

Modal identification usually adopts the state-space model shown in Equations (1)-(2). Here, $u_k \in \mathbb{R}^{n_i}$ (where n_i is the number of inputs) and $y_k \in \mathbb{R}^{n_o}$ (where n_o is the number of outputs) are the measured values for the input and output, respectively; $x_k \in \mathbb{R}^{n_x}$ (where n_x is the number of states) is the state vector; $w_k \in \mathbb{R}^{n_x}$ and $v_k \in \mathbb{R}^{n_o}$ are respectively the process noise and the measurement noise that are not measured; and, $A \in \mathbb{R}^{n_x \times n_x}$, $B \in \mathbb{R}^{n_x \times n_i}$, $C \in \mathbb{R}^{n_o \times n_x}$, $D \in \mathbb{R}^{n_o \times n_i}$ are respectively the state matrix, the input matrix, the output matrix and the direct feedthrough matrix. Since the external input is 0 ($u_k = 0$) for a stochastic system, B and D are unnecessary.

$$x_{k+1} = Ax_k + Bu_k + w_k \tag{1}$$

$$y_k = Cx_k + Du_k + v_k \tag{2}$$

The matrices A, (B), C, (D) forming the system can be obtained if modal identification is performed using the measured data y_k, (u_k). The eigenvalues ($\lambda_i \in \mathbb{R}$) and eigenvectors ($\phi_{yi} \in \mathbb{R}^{n_o}$) of the structure can be obtained by simple calculation [13] using these system matrices.

2.2. Measurement-model link

The eigenvector obtained by modal identification corresponds to that at the output measurement location. Besides, the eigenvector obtained by the analytic model is the one at the node DOF. In general, the output measurement location and the location of the node do not coincide, which means that these eigenvectors are at different locations. Moreover, the measurement direction is likely to

Preprints (www.preprints.org) | NOT PEER-REVIEWED | Posted: 3 September 2019 doi:10.20944/preprints201909.0034.v1

Peer-reviewed version available at Appl. Sci. 2019, 9, 4309; doi:10.3390/app9204309

differ from the DOF direction of the node. The type of eigenvector also differs between the measurement and the analytic model when the strain is measured. Accordingly, a solution is required to remedy the mismatch in the location, direction and type between the measurement and the analysis. To that goal, the relation between the node DOFs of the analytic model and the measured values shall be derived.

The analytic model can be placed in any arbitrary position in the space, and various sensors like accelerometers and strain gauges can be installed in each element of the analytic model (Figure 2). The spatial position in the analytic model is defined in the global coordinate system (GCS), and can be transformed into the element coordinate system (ECS). The location of the sensors and the measurement direction can be defined in GCS or ECS. The measurement direction $n = [n_x \quad n_y \quad n_z]^T$ in GCS is related to the measurement direction $n' = [n'_x \quad n'_y \quad n'_z]^T$ in ECS as follows.

$$n' = Rn \tag{3}$$

$$n = R^T n' \tag{4}$$

where the rotation matrix R is as follows.

$$R = \begin{bmatrix} \cos(x',x) & \cos(x',y) & \cos(x',z) \\ \cos(y',x) & \cos(y',y) & \cos(y',z) \\ \cos(z',x) & \cos(z',y) & \cos(z',z) \end{bmatrix} \tag{5}$$

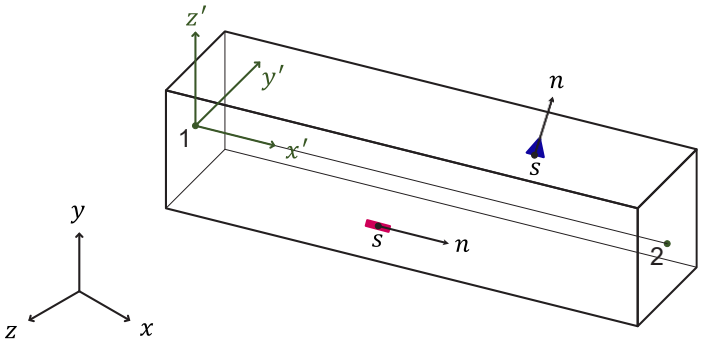

Figure 2. Relation between GCS and ECS.

2.2.1. Case where the displacement, velocity, acceleration are measured

The displacement d_n measured in the measurement direction n at the sensor location $s(s_x, s_y, s_z)$ satisfies the following relation with the displacement $d = [u \quad v \quad w]^T$ in GCS at the sensor location.

$$d_n = n^T d \tag{6}$$

where u, v, w are the displacements in directions x, y, z of GCS, respectively. The displacement d in GCS can be expressed in term of the displacement $d' = [u' \quad v' \quad w']^T$ in ECS.

$$d = R^T d' \tag{7}$$

where u', v', w' are the displacements in directions x', y', z' of ECS.

The displacement d' in ECS can be expressed as the product of the nodal displacement $\hat{d}'_e$ of the element and the shape function N_e.

$$d' = N_e \hat{d}'_e \tag{8}$$

The DOFs and shape functions of element vary according to the type of element used in the analytic model. The shape function for the 2-dimensional Euler-Bernoulli beam element is arranged in the Appendix.

The displacement $\hat{d}'_{eI}$ of the I-th node of the element can be represented as follows by distinguishing the translational DOFs and the rotational DOFs. Some DOFs may vanish according to the element type.

$$\hat{d}'_{eI} = \begin{bmatrix} \hat{u}'_I & \hat{v}'_I & \hat{w}'_I & \hat{\theta}'_{xI} & \hat{\theta}'_{yI} & \hat{\theta}'_{zI} \end{bmatrix}^T \tag{9}$$

$$\hat{d}'_e = [\cdots \quad \hat{d}'^T_{eI} \quad \cdots]^T \tag{10}$$

where $\hat{u}'_I, \hat{v}'_I, \hat{w}'_I$ are the translational DOFs in the x', y', z' directions of the I-th node; and, $\hat{\theta}'_{xI}, \hat{\theta}'_{yI}, \hat{\theta}'_{zI}$ are the rotational DOFs with respect to axes x', y', z' of the I-th node. The corresponding displacement $\hat{d}_{eI}$ of the I-th node in GCS can also be expressed similarly.

$$\hat{d}_{eI} = \begin{bmatrix} \hat{u}_I & \hat{v}_I & \hat{w}_I & \hat{\theta}_{xI} & \hat{\theta}_{yI} & \hat{\theta}_{zI} \end{bmatrix}^T \tag{11}$$

$$\hat{d}_e = [\cdots \quad \hat{d}^T_{eI} \quad \cdots]^T \tag{12}$$

where $\hat{u}_I, \hat{v}_I, \hat{w}_I$ are the translational DOFs in the x, y, z directions of the I-th node; and, $\hat{\theta}_{xI}, \hat{\theta}_{yI}, \hat{\theta}_{zI}$ are the rotational DOFs with respect to axes x, y, z of the I-th node. The node displacement $\hat{d}'_e$ in ECS satisfies the following relation with the node displacement $\hat{d}_e$ in GCS.

$$\hat{d}'_e = T\hat{d}_e \tag{13}$$

$$\hat{d}'_{eI} = T_I\hat{d}_{eI} = \begin{bmatrix} R & 0 \\ 0 & R \end{bmatrix} \hat{d}_{eI} \tag{14}$$

The displacement d_n in the measurement direction at the sensor location can be expressed by the node displacement in GCS using Equations (6)-(14).

$$d_n = \tilde{N}_e\hat{d}_e \tag{15}$$

where

$$\tilde{N}_e = n^T R^T N_e T = n'^T N_e T \tag{16}$$

The so-derived $\tilde{N}_e$ relates one sensor. Denoting $\tilde{N}_e$ for the i-th sensor by $\tilde{N}_{ei}$, matrix $\tilde{N}_d \in \mathbb{R}^{m_d \times n_d}$ (where m_d = number of displacement sensors, n_d = number of DOFs of analytic model) can be obtained for the whole set of displacement sensors by assembling the $\tilde{N}_{ei}$ as follows.

$$\tilde{N}_d = \sum_i^{m_d} \tilde{N}_{ei} \tag{17}$$

Matrices $\tilde{N}_v \in \mathbb{R}^{m_v \times n_d}$ (m_v = number of velocity sensors) and $\tilde{N}_a \in \mathbb{R}^{m_a \times n_d}$ (m_a = number of acceleration sensors) can be obtained using the same method for the velocity and the acceleration, respectively.

The displacement $d_s \in \mathbb{R}^{m_d}$, velocity $v_s \in \mathbb{R}^{m_v}$ and acceleration $a_s \in \mathbb{R}^{m_a}$ in the measurement direction and at the sensor location can be expressed in term of the node displacement $\hat{d} \in \mathbb{R}^{n_d}$, node velocity $\hat{v} \in \mathbb{R}^{n_d}$ and node acceleration $\hat{a} \in \mathbb{R}^{n_d}$ in GCS. Moreover, the displacement, velocity and acceleration can also be expressed in terms of the eigenvector $\phi_i \in \mathbb{R}^{n_d}$ and the generalized coordinates $q_{di}, q_{vi}, q_{ai} \in \mathbb{R}$ for the displacement, velocity and acceleration of the model as shown in Equations (18)-(20). In addition, the mode shapes $\phi_{dsi} \in \mathbb{R}^{m_d}$, $\phi_{vsi} \in \mathbb{R}^{m_v}$, $\phi_{asi} \in \mathbb{R}^{m_a}$ for the displacement, velocity and acceleration at the measurement location corresponding to eigenvector ϕ_i can be defined in terms of transformation matrices $\tilde{N}_d$, $\tilde{N}_v$, $\tilde{N}_a$ as shown in Equations (21)-(23).

$$d_s = \tilde{N}_d\hat{d} = \tilde{N}_d \sum_i^{n_d} \phi_i q_{di} = \sum_i^{n_d} \phi_{dsi} q_{di} \tag{18}$$

$$v_s = \tilde{N}_v\hat{v} = \tilde{N}_v \sum_i^{n_d} \phi_i q_{vi} = \sum_i^{n_d} \phi_{vsi} q_{vi} \tag{19}$$

$$a_s = \tilde{N}_a \hat{a} = \tilde{N}_a \sum_i^{n_d} \phi_i q_{ai} = \sum_i^{n_d} \phi_{asi} q_{ai} \tag{20}$$

where

$$\phi_{dsi} = \tilde{N}_d \phi_i \tag{21}$$

$$\phi_{vsi} = \tilde{N}_v \phi_i \tag{22}$$

$$\phi_{asi} = \tilde{N}_a \phi_i \tag{23}$$

2.2.2. Case where the strain is measured

The method derived in Section 0 can also be applied similarly for the strain. The strain ϵ_n measured at the sensor location $s(s_x, s_y, s_z)$ can be expressed in terms of the strain $\epsilon' = [\epsilon'_{xx} \quad \epsilon'_{yy} \quad \epsilon'_{zz} \quad \gamma'_{xy} \quad \gamma'_{yz} \quad \gamma'_{xz}]^T$ in ECS at the sensor location and the direction vector n' in ECS.

$$\epsilon_n = n'_x n'_x \epsilon'_{xx} + n'_y n'_y \epsilon'_{yy} + n'_z n'_z \epsilon'_{zz} + n'_x n'_y \gamma'_{xy} + n'_y n'_z \gamma'_{yz} + n'_x n'_z \gamma'_{xz} = (\tilde{n}')^T \epsilon' \tag{24}$$

where

$$\tilde{n}' = [n'_x n'_x \quad n'_y n'_y \quad n'_z n'_z \quad n'_x n'_y \quad n'_y n'_z \quad n'_x n'_z]^T \tag{25}$$

The strain ϵ' in ECS can be rewritten in term of the element node displacement $\hat{d}'_e$ using the displacement-strain transform matrix B_e.

$$\epsilon' = B_e \hat{d}'_e \tag{26}$$

Matrix B_e also varies according to the element type. The displacement-strain transform matrix for the 2-dimensional Euler-Bernoulli beam element is arranged in the Appendix. Following the process formulated in Equations (9)-(14), the strain ϵ_n in the measurement direction and at the sensor location can be expressed in term of the node displacement in GCS.

$$\epsilon_n = \tilde{B}_e \hat{d}_e \tag{27}$$

where

$$\tilde{B}_e = (\tilde{n}')^T B_e T \tag{28}$$

The so-derived matrix $\tilde{B}_e$ relates one strain gauge. Denoting $\tilde{B}_e$ for the i-th sensor by $\tilde{B}_{ei}$, matrix $\tilde{B} \in \mathbb{R}^{m_\epsilon \times n_d}$ (m_ϵ = number of strain gauges) can be obtained for the whole set of sensors by assembling the $\tilde{B}_{ei}$ as follows.

$$\tilde{B} = \sum_i^{m_\epsilon} \tilde{B}_{ei} \tag{29}$$

The strain $\epsilon_s \in \mathbb{R}^{m_\epsilon}$ in the measurement direction at the sensor location can be expressed by means of the node displacement $\hat{d} \in \mathbb{R}^{n_d}$ in GCS using this process. Moreover, the strain ϵ_s can be expressed by means of the eigenvector ϕ_i defined at the node DOF or the mode shape $\phi_{\epsilon si} \in \mathbb{R}^{m_\epsilon}$ for the strain at the measurement location as shown in Equations (30), (31).

$$\epsilon_s = \tilde{B} \hat{d} = \tilde{B} \sum_i^{n_d} \phi_i q_{di} = \sum_i^{n_d} \phi_{\epsilon si} q_{di} \tag{30}$$

where

$$\phi_{\epsilon si} = \tilde{B} \phi_i \tag{31}$$

The above process makes it possible to express the measured displacement, velocity, acceleration and strain in terms of the node DOFs of the model. Moreover, the mode shapes ϕ_{dsi}, ϕ_{vsi}, ϕ_{asi}, $\phi_{\epsilon si}$ for the measured values corresponding to the eigenvector ϕ_i of the node DOFs are also defined. The

transform matrices $\tilde{N}$ and $\tilde{B}$ bridging the measurement and the analysis were derived solely using geometrical relations and will thus applicable as they are even in case of change in the material characteristics. For convenience in the following, ϕ_{si} will denote the mode shape for the measured value and $\tilde{S}$ will denote the transform matrix to reduce Equations (21)-(23), (31) into the unique form expressed hereafter.

$$\phi_{si} = \tilde{S}\phi_i \tag{32}$$

2.3. Model updating

Model updating is the process by which the model parameters are updated using the measured data to make the numerical model behave as close as possible like the actual structure. The mode shape vector used during this process is the mode shape vector related to the node DOF. This is in contrast with the mode shape vector obtained by modal identification in relation with the physical quantities measured at the location and direction of the sensors. These two mode shape vectors have thus different forms. Accordingly, a method to make them fit to each other is necessary. Among them, the model updating using the sensitivity method [5] is explained.

The basic formulation of model updating is as follows.

$$\min|z_{mea} - z(\theta)| \tag{33}$$

where z_{mea}, $z(\theta) \in \mathbb{R}^{n_z}$ (n_z = number of compared variables) are the values obtained respectively by measurement and by analysis; and, $\theta \in \mathbb{R}^{n_\theta}$ (n_θ = number of model parameters) is the model parameter to be updated. This equation can be reformulated as follows for sensitivity analysis.

$$\min|r^k - G^k \Delta\theta^k| \tag{34}$$

with

$$r^k = z_{mea} - z(\theta^k) \tag{35}$$

$$G^k = \left[\frac{\partial z_i}{\partial \theta_j}\right]_{\theta=\theta^k} \tag{36}$$

where k is the number of iteration; $r^k \in \mathbb{R}^{n_z}$ is the residual; and, $G^k \in \mathbb{R}^{n_z \times n_\theta}$ is the sensitivity matrix. The iteration proceeds by solving Equation (34) for $\Delta\theta^k$ to obtain $\theta^{k+1} = \theta^k + \Delta\theta^k$ of the next step until convergence.

The i-th eigenvalue $\lambda_i \in \mathbb{R}$ and eigenvector $\phi_i \in \mathbb{R}^{n_d}$ of the analytic model are obtained from the stiffness matrix $K(\theta)$ and the mass matrix $M(\theta)$.

$$K(\theta)\phi_i = \lambda_i M(\theta)\phi_i \tag{37}$$

2.3.1. Eigenvalue residual

Being a behavioral characteristic of the entire structure, the eigenvalue is practically not affected by the location nor the type of sensor. However, the analytic mode shall be paired to its corresponding measured mode by the modal assurance criterion (MAC) [14] in order to compare the eigenvalue for the same mode. In such mode pairing, the analytic mode shape compared to the measured mode shape $\phi_{i,mea}$ shall be $\phi_{sj}(=\tilde{S}\phi_j)$, $j = 1, \cdots, n_d$ obtained by Equation (32) and not be ϕ_j.

Once the analytic mode corresponding to the measured mode is obtained, the residual and sensitivity matrices can be constructed as follows [15].

$$r^k = \lambda_{i,mea} - \lambda_i(\theta^k) \tag{38}$$

Preprints (www.preprints.org) | NOT PEER-REVIEWED | Posted: 3 September 2019 doi:10.20944/preprints201909.0034.v1

Peer-reviewed version available at Appl. Sci. 2019, 9, 4309; doi:10.3390/app9204309

$$\frac{\partial \lambda_i}{\partial \theta_j} = \phi_i^T \left(-\lambda_i \frac{\partial M}{\partial \theta_j} + \frac{\partial K}{\partial \theta_j} \right) \phi_i \tag{39}$$

where $M, K \in \mathbb{R}^{n_d \times n_d}$ are the mass and stiffness matrices of the analytic model; and, λ_i, ϕ_i are the i-th eigenvalue and eigenvector. Here, the eigenvector shall be normalized for the mass matrix.

2.3.2. Mode shape residual

The mode pairing shall be performed by the method explained in section 0 to make the comparison between corresponding modes. In addition, the measured mode shape $\phi_{i,mea}$ and the analytic mode shape $\phi_{si}(= \tilde{S}\phi_i)$ that have been paired may differ by a definite ratio and shall thus be scaled by an appropriate method.

Mode scaling can be done for the measurement mode shape as well as for the analysis mode shape. Here, the measurement mode shape is scaled with respect to the analysis mode shape. The scaled measurement mode shape $\phi_{si,mea}$ can be obtained as follows using the modal scale factor (MSF) [14] of the analytic mode shape ϕ_{si} for the measured mode shape $\phi_{i,mea}$.

$$\phi_{si,mea} = MSF(\phi_{si}, \phi_{i,mea})\phi_{i,mea} \tag{40}$$

where

$$MSF(\phi_{si}, \phi_{i,mea}) = \frac{\phi_{si}^T \phi_{i,mea}^*}{\phi_{i,mea}^T \phi_{i,mea}^*} \tag{41}$$

Once the scaled measurement mode shape is obtained, the residual and sensitivity matrices can be constructed as follows.

$$r^k = \phi_{si,mea} - \phi_{si}(\theta^k) \tag{42}$$

$$\frac{\partial \phi_{si}}{\partial \theta_j} = \frac{\partial (\tilde{S}\phi_i)}{\partial \theta_j} = \tilde{S}\frac{\partial \phi_i}{\partial \theta_j} \tag{43}$$

where the derivative $\frac{\partial \phi_i}{\partial \theta_j}$ with respect to the eigenvector can be obtained by previous studies [15,16]. The method of Fox and Kapoor [15] necessitates the whole eigenvectors to obtain the derivative for the i-th eigenvector whereas the method of Nelson [16] provides higher calculation efficiency since it uses only the i-th eigenvector to obtain the derivative.

3. Numerical example

The simple numerical example shown in Figure 3 is adopted to explain numerically the method described in Section 2. The structure is a simply supported beam of 15 m with a height of 1 m and width of 0.5 m. The beam is modeled by 2-dimensional Euler-Bernoulli beam elements. The elastic modulus is 25 GPa, the Poisson's ratio is 0.2 and the density is 2,300 kg/m^3. The structural damping ratio for the 1st and 2nd modes is 5%. Strain gauges are installed longitudinally in the center of each element at height of 50 mm from the bottom and accelerometers are installed vertically at the top of the center of each element.

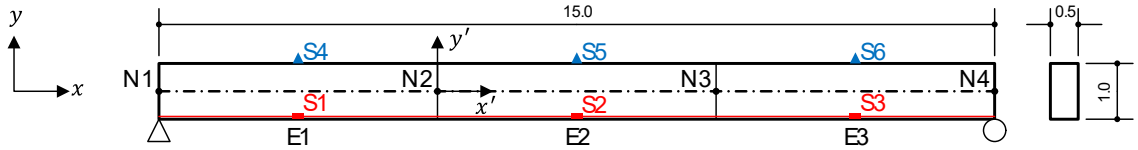

Figure 3. Structure shape and sensor layout of numerical example (unit: m)

3.1. Modal identification

Data measured by sensors are needed for modal identification but were generated analytically here. An initial velocity of –0.1 m/s was given vertically to nodes 2 and 3 in the model shown in Figure 3 to obtain the time histories of the displacement and acceleration at the sensor locations. These generated values were then adopted as measured data to perform modal identification, which provided the mode shape $\phi_{\epsilon i,mea}$ for the strain, the mode shape $\phi_{ai,mea}$ for the acceleration and the eigenvalue $\lambda_{i,mea}$. For simplification, only the first mode was considered. For the first mode, λ_{mea} = 1738.8 and the mode shapes for the strain and the acceleration are as follows.

$$\phi_{\epsilon,mea} = \phi_{a,mea} = [0.408 \quad 0.816 \quad 0.408]^T \tag{44}$$

3.2. Construction of transform matrices

Since GCS and ECS coincide, the rotation matrix R is the identity matrix. The measurement direction of the strain gauges is $n_{S1} = n_{S2} = n_{S3} = [1.0 \quad 0.0]^T$, and the measurement direction ($n' = Rn$) in ECS becomes $n'_{S1} = n'_{S2} = n'_{S3} = [1.0 \quad 0.0]^T$. The measurement direction of the accelerometers is $n_{S4} = n_{S5} = n_{S6} = [0.0 \quad 1.0]^T$ and is $n'_{S1} = n'_{S2} = n'_{S3} = [0.0 \quad 1.0]^T$ in ECS.

The strain components of the 2-dimensional Euler-Bernoulli beam element are the longitudinal strain component (ϵ'_{xx}) and the transverse strain component (ϵ'_{yy}) induced by the Poisson's effect. Matrix B_{ei}, which relates the strain ($\epsilon' = [\epsilon'_{xx} \quad \epsilon'_{yy}]^T$) of the element and the displacement ($\hat{d}'_e = [\hat{u}'_1 \quad \hat{v}'_1 \quad \hat{\theta}'_1 \quad \hat{u}'_2 \quad \hat{v}'_2 \quad \hat{\theta}'_2]^T$) of the node (subscripts 1 and 2 indicate respectively the first and second nodes of the element), can be obtained as follows using Equation (56).

$$B_{e1} = B_{e2} = B_{e3} = \begin{bmatrix} 0.2 & 0.0 & -0.09 & 0.2 & 0.0 & 0.09 \\ -0.04 & 0.0 & 0.018 & -0.04 & 0.0 & -0.018 \end{bmatrix} \tag{45}$$

Transforming B_{ei} into $\tilde{B}_{ei}$, which relates the node and measurement directions in GCS, gives

$$\tilde{B}_{e1} = \tilde{B}_{e2} = \tilde{B}_{e3} = [0.2 \quad 0.0 \quad -0.09 \quad 0.2 \quad 0.0 \quad 0.09] \tag{46}$$

Assembling the transform matrices obtained for the strain gauges with respect to the global DOFs provides the transform matrix $\tilde{B}$ for the whole set of strain gauges.

$$\phi_{\epsilon s} = \tilde{B}\phi \tag{47}$$

where

$$\phi = [\phi_{\hat{u}_1} \quad \phi_{\hat{v}_1} \quad \phi_{\hat{\theta}_1} \quad \phi_{\hat{u}_2} \quad \phi_{\hat{v}_2} \quad \phi_{\hat{\theta}_2} \quad \phi_{\hat{u}_3} \quad \phi_{\hat{v}_3} \quad \phi_{\hat{\theta}_3} \quad \phi_{\hat{u}_4} \quad \phi_{\hat{v}_4} \quad \phi_{\hat{\theta}_4}]^T \tag{48}$$

$$\tilde{B} = \begin{bmatrix} -0.2 & 0.0 & -0.09 & 0.2 & 0.0 & 0.09 & 0.0 & 0.0 & 0.0 & 0.0 & 0.0 & 0.0 \\ 0.0 & 0.0 & 0.0 & -0.2 & 0.0 & -0.09 & 0.2 & 0.0 & 0.09 & 0.0 & 0.0 & 0.0 \\ 0.0 & 0.0 & 0.0 & 0.0 & 0.0 & 0.0 & -0.2 & 0.0 & -0.09 & 0.2 & 0.0 & 0.09 \end{bmatrix} \tag{49}$$

In Equation (48), $\phi_{\hat{u}_1}$, $\phi_{\hat{v}_1}$, $\phi_{\hat{v}_4}$ corresponding to the fixed DOFs are 0 and can thus be discarded.

The displacement components of the 2-dimensional Euler-Bernoulli beam element are the longitudinal component (u') and the transverse component (v'). Matrix N_{ei}, which relates the element displacement ($d' = [u' \quad v']^T$) and the node displacement can be obtained as follows using Equation (59).

$$N_{e4} = N_{e5} = N_{e6} = \begin{bmatrix} 0.5 & 0.15 & 0.125 & 0.5 & -0.15 & 0.125 \\ 0.0 & 0.5 & 0.625 & 0.0 & 0.5 & -0.625 \end{bmatrix} \tag{50}$$

Transforming N_{ei} into $\tilde{N}_{ei}$, which relates the DOFs of GCS and the displacement in the measurement direction, gives

$$\tilde{N}_{e4} = \tilde{N}_{e5} = \tilde{N}_{e6} = [0.0 \quad 0.5 \quad 0.625 \quad 0.0 \quad 0.5 \quad -0.625] \tag{51}$$

Assembling the transform matrices obtained for the accelerometers with respect to the global DOFs provides the transform matrix $\tilde{N}_a$ for the whole set of accelerometers.

Preprints (www.preprints.org) | NOT PEER-REVIEWED | Posted: 3 September 2019 doi:10.20944/preprints201909.0034.v1

Peer-reviewed version available at Appl. Sci. 2019, 9, 4309; doi:10.3390/app9204309

$$\phi_{as} = \tilde{N}_a \phi \tag{52}$$

where

$$\tilde{N}_a = \begin{bmatrix} 0.0 & 0.5 & 0.625 & 0.0 & 0.5 & -0.625 & 0.0 & 0.0 & 0.0 & 0.0 & 0.0 & 0.0 \\ 0.0 & 0.0 & 0.0 & 0.0 & 0.5 & 0.625 & 0.0 & 0.5 & -0.625 & 0.0 & 0.0 & 0.0 \\ 0.0 & 0.0 & 0.0 & 0.0 & 0.0 & 0.0 & 0.0 & 0.5 & 0.625 & 0.0 & 0.5 & -0.625 \end{bmatrix} \tag{53}$$

3.3. Model updating

As explained in section 0, the model updating process is practically similar to previous model updating methods. The difference is that the mode shape of the node DOF of Equation (37) is not used as it is but is transformed into the measured values as shown in Equations (42) and (43) when the residual for the mode shape is adopted as objective function.

Model updating can be done for the measurement mode obtained from the strain sensors or for the measurement mode obtained from the acceleration sensors or for the mixed measurement mode from both types of sensors. Since model updating for the mixed measurement mode falls out of the scope of the present study, this case is not considered here.

Under the assumption that the initial elastic modulus of all the elements is 20 GPa, the model updating using the eigenvalue λ_{mea} of the strain gauges, the measured mode $\phi_{\epsilon,mea}$ and the transform matrix $\tilde{B}$ gives an elastic modulus of 25 GPa for all the elements. This value corresponds to that of the model and demonstrates the feasibility of the proposed approach. In addition, the model updating using the eigenvalue λ_{mea} of the accelerometers, the measured mode $\phi_{a,mea}$ and the transform matrix $\tilde{N}_a$ provides similar results.

The proposed approach is seen to allow model updating not only by means of the acceleration measurement but also by means of the strain measurement. There is also no need to limit the location of the sensors to the location of the nodes in the model. This means that the sensors can be installed at arbitrary locations inside the structure. Consequently, it is now possible to model the structure regardless of the position of the sensors and to select the location of the sensors independently from the model.

4. Numerical Application to Bridge

In order to verify the applicability of the proposed approach for large scale structures, the numerical example shown in Figure 4 is established. The structure is a prestressed concrete box girder bridge with length of 50 m, height of 3 m and width of 16.8 m. The bridge is composed of 19 segments and the material density is 2,500 kg/m^3. The damping ratio for the 1st and 2nd modes is 5%. A total of 50 strain sensors are installed longitudinally along the section bottom centerline at spacing of 1 m. This sensor layout can be achieved one fiber optic sensor using the quasi-distributed fiber optic sensor [17] based on the resonance frequency mapping.

The structure is modeled using 556 4-node shell elements giving a total of 569 nodes and 3,414 DOFs. Identical elastic modulus is assumed for the elements inside each segment. Except segments No. 6 and No. 11, the elastic modulus of the segments is 30 GPa and is set to a value of 27 GPa for segments No. 6 and No. 11 with 10% damage. The eigenvalue analysis of the structure gave a natural frequency of 2.083Hz for the 1st mode. The mode shape is shown in Figure 4(d).

Preprints (www.preprints.org) | NOT PEER-REVIEWED | Posted: 3 September 2019 doi:10.20944/preprints201909.0034.v1

Peer-reviewed version available at Appl. Sci. 2019, 9, 4309; doi:10.3390/app9204309

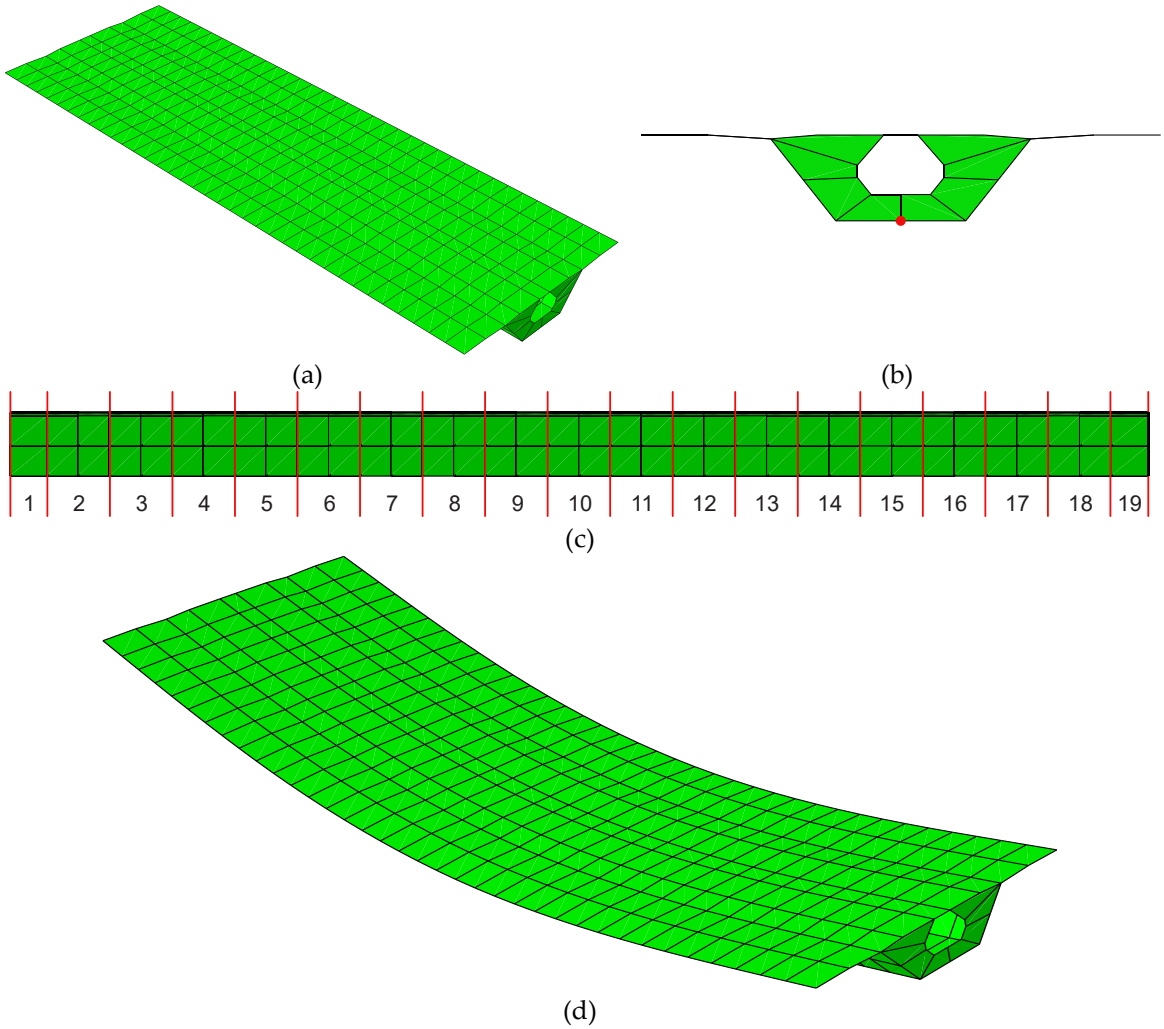

Figure 4. Numerical application (a) shape of bridge structure, (b) layout of strain sensors, (c) segments of structure, (d) first mode shape of structure.

An arbitrary load was applied vertically on the upper side of the structure and the strain was measured at sampling rate of 100 Hz during 100 seconds. Figure 5(a) plots the strains measured by the 50 sensors. The modal identification for the measured strains gives the mode shape shown in Figure 5(b). Here, the analytic solution was obtained directly from the mass and stiffness matrices of the structure. The mode shape obtained from the modal identification is seen to approach the analytic solution. The natural frequency for the mode at hand is 2.065 Hz and shows an error of merely 0.86% compared to the analytic solution (2.083 Hz).

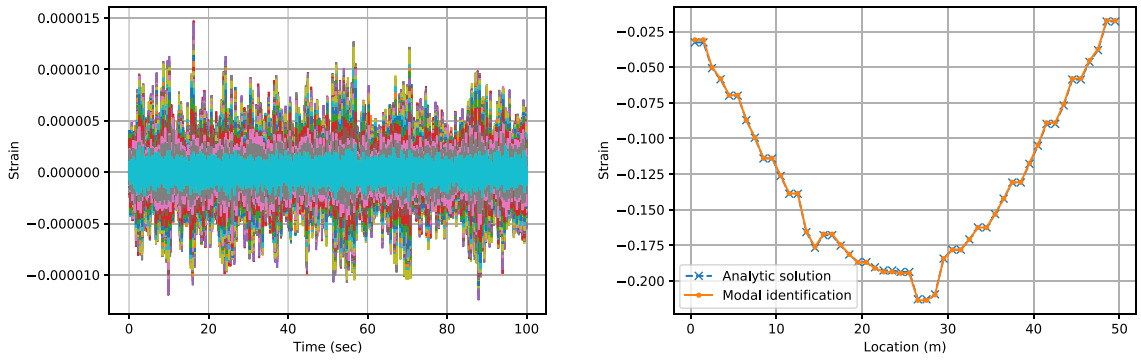

(a) (b)

Figure 5. Modal identification (a) measured strains; (b) mode shape obtained by modal identification.

Preprints (www.preprints.org) | NOT PEER-REVIEWED | Posted: 3 September 2019 doi:10.20944/preprints201909.0034.v1

Peer-reviewed version available at Appl. Sci. 2019, 9, 4309; doi:10.3390/app9204309

The elastic modulus of the model can be obtained by model updating using the eigenvalue and strain measurement mode shape provided by the modal identification. Figure 6(a) compares the elastic moduli of the updated model with those of the structure and shows good agreement. Figure 6(b) plots the error ratio of the structure-updated model elastic moduli and reveals a maximum error of about 4%, which demonstrates that the model was fairly updated.

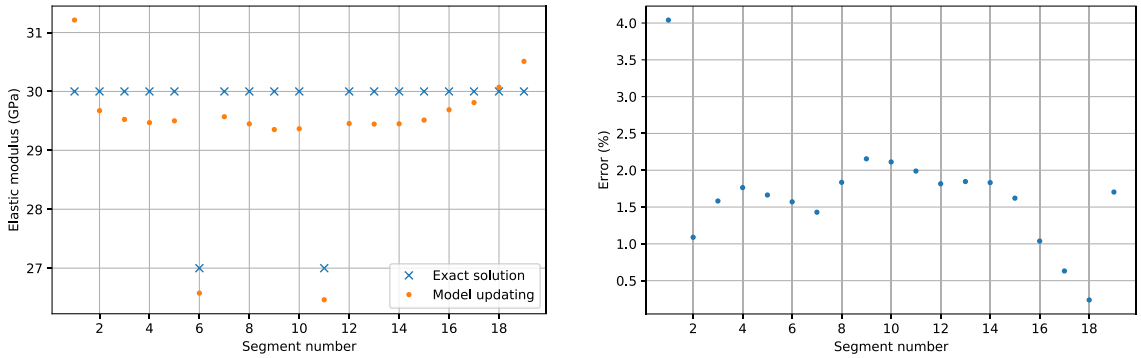

(a) (b)

Figure 6. Model updating results (a) comparison of elastic moduli of structure and updated model; (b) error ratio of structure-updated model elastic moduli.

In addition, the model updating using the eigenvalue and the strain measurement mode shape of the structure instead of the eigenvalue and the measurement mode shape obtained by modal identification resulted in elastic moduli identical to the exact solution of Figure 6(a). This shows that the error observed in the model updating was generated during the modal identification process.

5. Conclusion

A systematic approach using the modal identification results in model updating was proposed. The mode shape obtained by modal identification and the mode shape of the model updating process do not coincide even for the same mode. A method constructing transform matrices considering the cases where the measurement is done by acceleration, velocity and displacement sensors and the case where the measurement is achieved by strain sensors was proposed to remedy this disagreement between these mode shapes. The constructed transform matrices are applied when the mode shape residual is used as objective function and for the mode pairing in the model updating process. The feasibility of the proposed approach was demonstrated through numerical examples involving strain or acceleration measurement. The proposed approach allows the sensors be disposed at locations representing appropriately the behavior of interest since the layout and direction of the sensors are not limited by the meshing of the model.

Author Contributions: Conceptualization, K. Cho and J.-R. Cho; methodology, K. Cho; software, K. Cho; validation, K. Cho; writing—original draft preparation, K. Cho; writing—review and editing, J.-R. Cho and Y.-H. Park; project administration, Y.-H. Park; funding acquisition, Y.-H. Park.

Acknowledgments: This research was funded by Korea Institute of Civil Engineering and Building Technology, grant from a Strategic Research Project (Smart Monitoring System for Concrete Structures Using FRP Nerve Sensor).

Conflicts of Interest: The authors declare no conflict of interest.

Appendix A Two-dimensional Euler-Bernoulli beam element

As shown in Figure 7, the 2-dimensional Euler-Bernoulli beam element has two nodes with the DOFs of Equation (54).

Preprints (www.preprints.org) | NOT PEER-REVIEWED | Posted: 3 September 2019 doi:10.20944/preprints201909.0034.v1

Peer-reviewed version available at Appl. Sci. 2019, 9, 4309; doi:10.3390/app9204309

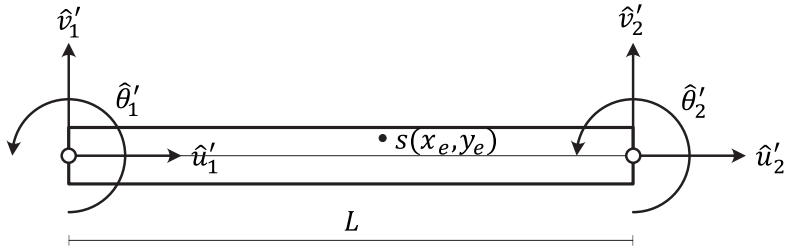

Figure 7. DOFs of 2-dimensional beam element.

$$\hat{d}_e' = [\hat{u}_1' \quad \hat{v}_1' \quad \hat{\theta}_1' \quad \hat{u}_2' \quad \hat{v}_2' \quad \hat{\theta}_2']^T \tag{54}$$

The strain ϵ' at an arbitrary position in the element is formed by the longitudinal strain ϵ_{xx}' and the strain ϵ_{yy}' generated by the Poisson's effect.

$$\epsilon' = [\epsilon_{xx}' \quad \epsilon_{yy}']^T \tag{55}$$

Matrix B_e relating the node DOF $\hat{d}_e'$ of the element with the strain ϵ' at an arbitrary position in the element is as follows.

$$B_e = \begin{bmatrix} B_{xx} \\ -\nu B_{xx} \end{bmatrix} \tag{56}$$

where

$$B_{xx} = \left[-\frac{1}{L} \quad -y_e\left(-\frac{6}{L^2}+\frac{12x_e}{L^3}\right) \quad -y_e\left(-\frac{4}{L}+\frac{6x_e}{L^2}\right) \quad \frac{1}{L} \quad -y_e\left(\frac{6}{L^2}-\frac{12x_e}{L^3}\right) \quad -y_e\left(-\frac{2}{L}+\frac{6x_e}{L^2}\right)\right] \tag{57}$$

The displacement d' at an arbitrary position in the element is formed by the longitudinal displacement u' and the transverse displacement v'.

$$d' = [u' \quad v']^T \tag{58}$$

Matrix N_e relating the node DOF $\hat{d}_e'$ of the element and the displacement d' at an arbitrary position in the element is as follows.

$$N_e = \begin{bmatrix} 1-\frac{x_e}{L} & -y_e\left(-\frac{6x_e}{L^2}+\frac{6x_e^2}{L^3}\right) & -y_e\left(1-\frac{4x_e}{L}+\frac{3x_e^2}{L^2}\right) & \frac{x_e}{L} & -y_e\left(\frac{6x_e}{L^2}-\frac{6x_e^2}{L^3}\right) & -y_e\left(-\frac{2x_e}{L}+\frac{3x_e^2}{L^2}\right) \\ 0 & 1-\frac{3x_e^2}{L^2}+\frac{2x_e^3}{L^3} & x_e-\frac{2x_e^2}{L}+\frac{x_e^3}{L^2} & 0 & \frac{3x_e^2}{L^2}-\frac{2x_e^3}{L^3} & -\frac{x_e^2}{L}+\frac{x_e^3}{L^2} \end{bmatrix} \tag{59}$$

References

1. Brincker, R.; Zhang, L.; Andersen, P. In Modal identification from ambient responses using frequency domain decomposition, Proc. of the 18*'International Modal Analysis Conference (IMAC), San Antonio, Texas, 2000.
2. Juang, J.-N.; Pappa, R.S. An eigensystem realization algorithm for modal parameter identification and model reduction. Journal of guidance, control, and dynamics 1985, 8, 620-627.
3. Qin, S.J. An overview of subspace identification. Computers & chemical engineering 2006, 30, 1502-1513.
4. Van Overschee, P.; De Moor, B. Subspace identification for linear systems: Theory—implementation—applications. Springer Science & Business Media: 2012.
5. Mottershead, J.E.; Link, M.; Friswell, M.I. The sensitivity method in finite element model updating: A tutorial. Mechanical Systems and Signal Processing 2011, 25, 2275-2296.

6. Mottershead, J.E.; Friswell, M.I. Model updating in structural dynamics: A survey. Journal of Sound and Vibration 1993, 167, 347-375.
7. Yuen, K.-V. Bayesian methods for structural dynamics and civil engineering. John Wiley & Sons: 2010.
8. Katafygiotis, L.S.; Beck, J.L. Updating models and their uncertainties. Ii: Model identifiability. Journal of Engineering Mechanics 1998, 124, 463-467.
9. Beck, J.L.; Katafygiotis, L.S. Updating models and their uncertainties. I: Bayesian statistical framework. Journal of Engineering Mechanics 1998, 124, 455-461.
10. Mares, C.; Mottershead, J.; Friswell, M. Stochastic model updating: Part 1—theory and simulated example. Mechanical Systems and Signal Processing 2006, 20, 1674-1695.
11. Sanayei, M.; Saletnik, M.J. Parameter estimation of structures from static strain measurements. I: Formulation. Journal of Structural Engineering 1996, 122, 555-562.
12. Esfandiari, A.; Sanayei, M.; Bakhtiari-Nejad, F.; Rahai, A. Finite element model updating using frequency response function of incomplete strain data. AIAA journal 2010, 48, 1420-1433.
13. Reynders, E.; Roeck, G.D. Reference-based combined deterministic–stochastic subspace identification for experimental and operational modal analysis. Mechanical Systems and Signal Processing 2008, 22, 617-637.
14. Allemang, R.J. The modal assurance criterion–twenty years of use and abuse. Sound and vibration 2003, 37, 14-23.
15. Fox, R.; Kapoor, M. Rates of change of eigenvalues and eigenvectors. AIAA journal 1968, 6, 2426-2429.
16. Nelson, R.B. Simplified calculation of eigenvector derivatives. AIAA journal 1976, 14, 1201-1205.
17. Kim, G.H.; Park, S.M.; Park, C.H.; Jang, H.; Kim, C.-S.; Lee, H.D. Real-time quasi-distributed fiber optic sensor based on resonance frequency mapping. Sci Rep-Uk 2019, 9, 3921.